

## 3D Imaging of Fine Needle Aspirates Using Optical Projection Tomographic Microscopy

Kenny F Chou<sup>1</sup>, Qin Miao<sup>2</sup>, Ryan L Coe<sup>1</sup> and Eric J Seibel<sup>3\*</sup>

<sup>1</sup>Department of Bioengineering, University of Washington, Seattle, WA 98105, USA

<sup>2</sup>Department of Mechanical Engineering, Massachusetts Institute of Technology, Cambridge, MA 02139, USA

<sup>3</sup>Human Photonics Lab, Department of Mechanical Engineering, University of Washington, Seattle, WA 98105, USA

### Abstract

Conventional Fine Needle Aspiration Biopsy (FNAB) requires minimal tissue sampling and causes minor tissue trauma. For these reasons, it is widely used to diagnose many types of cancers. However, the utility of FNA is limited, due to the lack of sensitivity and loss of structural information. This preliminary study introduces a new type of Three-Dimensional (3D) cytological imaging, Optical Projection Tomographic Microscopy (OPTM) that has the potential to reduce errors in FNAB analysis. We first demonstrate the functionality of OPTM, a microscopic imaging method that produces high resolution 3D images of single cell specimens in absorption mode, to perform multi-cellular imaging of cells stained with hematoxylin. Then, we use OPTM to image entire FNAB-like specimens in their three-dimensional form without experiencing errors from overlapping cells, choice of focal plane, and sampling. Our methods show success in generating volumetric data of large density of cells inside a cylindrical tube representative of FNA specimen within a 23-gauge needle. This 3D imaging technique may be applied to thin core needlebiopsyspecimens in the future, which may allow the preservation of tissue microstructure in FNAB specimens.

**Keywords:** Optical Projection Tomographic Microscopy (OPTM); Fine Needle Aspiration (FNA)

### Introduction

FNA is an established minimally-invasive technique to obtain biopsy specimens. Diagnostic FNA samples from thyroid nodules have drastically reduced the need for diagnostic thyroidectomy [1]. However, FNA biopsy reliability is not 100%; diagnosis of surface tissue lesions yields sensitivity and specificity ranging from 0.86 – 0.98 and 0.94–1.0, respectively, depending on the location sampled [2-6]. Diagnostic accuracy of endoscopically guided FNA is much lower, between 0.6–0.9 [7-10]. It had been shown that combining histology with cytology can improve diagnostic accuracy and overcome the limitation in the amount and type of information that cytology alone can provide [11-13]. For example, tissue structure shown in histology allows pathologists to identify the organization of neoplastic cells with respect to each other, presence or absence of basement membranes, quality and type of supporting connective tissue, including blood vessels, and the invasive relationship between tumor cells and these structures. The amount of information gained from histology has often led to a change in the diagnostic outcome [12,14,15]. Unfragmented tissue samples are typically obtained from Core Needle Biopsy (CNB), which uses a larger diameter needle (e.g. 14 G, 2.1 mm OD, 1.6 mm ID), making it much more invasive than FNA, which uses smaller diameter needles (e.g. 22 G, 0.718 mm OD, 0.413 mm ID). This larger sized CNB specimen is too large to observe at high resolution on a bright field optical microscope, requiring additional tissue slice sampling to be performed.

A typical FNA sample yields 75,000 cells [1]. Given the physical demand and time requirement needed, it is difficult to examine all cells aspirated from FNA with conventional 2D cytology. Clinicians select a sample of FNA for analysis, occasionally resulting in inadequate sampling [5,8]. Attempting to isolate cells from tissue fragments can damage the sample, also contributing to diagnostic errors. These errors may be eliminated if entire FNA samples can be imaged in their original Three-Dimensional (3D) form. In addition, issues with cell overlap

and optical focal plane are not present in 3D imaging. Therefore, 3D imaging allows tissue fragments in the aspirates to be analyzed, which may yield additional morphological information otherwise unavailable with 2D cytology.

Well-known 3D microscopy methods such as confocal microscopy produce anisotropic images [16] and rely on fluorescence contrast in the epi-illumination mode [17-19]. These methods are unsuitable for clinical use, since conventional FNA and CNB samples are imaged using absorptive stains, e.g. Hematoxylin and Eosin (H&E) stain, in optical transmission mode. To overcome these obstacles, a new technique to form 3D images in transmission mode, called Optical Projection Tomographic Microscopy (OPTM), has been developed to produce isotropic, high resolution images of cells with absorptive stain, such as hematoxylin [20]. Compared to using 2D analysis used today, single cell analysis by OPTM in 3D has been demonstrated to reduce false-negative rate in adenocarcinoma detection by threefold [21]. OPTM is currently designed to image single cells but can be extended to image multicellular and tissue fragment specimens [22]. This study extends the functionality of OPTM to perform multi-cellular imaging and shows the possibility of whole-FNA imaging using OPTM as a way to reduce errors in FNA diagnosis. Simulated FNA specimens are used in this preliminary report using a prototype OPTM instrument, with discussion on future applicability of imaging entire FNA and CNB specimens from tissue.

**\*Corresponding author:** Eric J Seibel, Human Photonics Lab, Department of Mechanical Engineering, University of Washington, Seattle, WA 98105, USA, Tel: 206-616-1486; E-mail: [eseibel@u.washington.edu](mailto:eseibel@u.washington.edu)

**Received** August 15, 2012; **Accepted** August 28, 2012; **Published** August 30, 2012

**Citation:** Chou KF, Miao Q, Coe RL, Seibel EJ (2012) 3D Imaging of Fine Needle Aspirates Using Optical Projection Tomographic Microscopy. J Cytol Histol S2:001. doi:10.4172/2157-7099.S2-001

**Copyright:** © 2012 Chou KF, et al. This is an open-access article distributed under the terms of the Creative Commons Attribution License, which permits unrestricted use, distribution, and reproduction in any medium, provided the original author and source are credited.

## Materials and Methods

### Specimen preparation

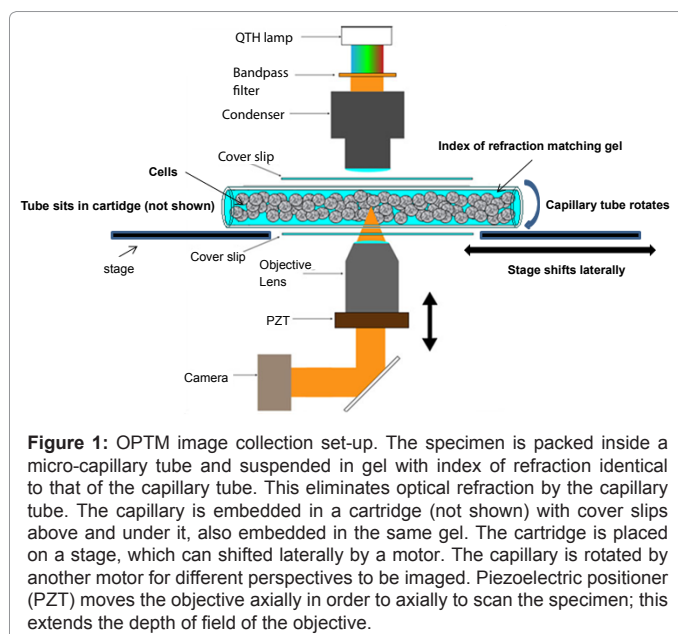
Indian Muntjac cells (a fibroblast cell line derived from epidermis of the Indian Muntjac deer) are prepared as described by Miao et al. [23] to form artificial tissue constructs within a capillary tube. Chicken red blood cell (RBC) nuclei are also prepared with the same method. A suspension of fixed and stained cells in optical gel (Nye OC431A-LVP, Nye Lubricants, MA) is injected from a syringe (Hamilton, NV) into a fused-silica capillary (Polymicro technologies, AZ) [23]. The capillary is embedded within a custom-made cartridge, which allows the capillary tube to be rotated, and fits onto the OPTM stage for imaging.

4.1.2 OPTM imaging: The OPTM platform and method for single cellular imaging, and the additional modes of biomarker fluorescence and nanoparticle scattering contrast is well documented [24]. Several changes are made to the OPTM to perform multi-cellular imaging; a schematic is shown in Figure 1. Depending on the size of the micro capillary housing the sample, the objective power and Numerical Aperture (NA) is decreased accordingly to increase the field of view (FOV), as recorded in Table 1.

A piezoelectric positioner (MIPOS-500, Piezosystem Jena) is used to axially move the objective and extend the system's depth of field. Similar to single-cell imaging, the capillary tube is rotated a full 360 degrees in 0.72 degree increments, and a projection image is obtained at each of the 500 perspectives. However, the simulated FNA specimen may extend beyond a single field of view along both x- and y- axes. Therefore, after a full capillary rotation, a motor shifts the stage laterally along either x- or y- axis in order to image the next section of the specimen. This step is repeated until the entire sample is imaged. In this particular experiment, images are captured on a grey-scale CCD camera (DL604M-OEM, Andor, Belfast, Ireland).

### 3D Image formation and processing

Image processing comprises three steps: registration (alignment) of the projections from each perspective, removal of the background pixels, and 3D reconstruction. Background removal is necessary to



Objective power	Manufacturer	NA	FOV ( $\mu\text{m}$ )	Capillary size ( $\mu\text{m}$ , inner diameter)	Image specimen	Cell specimen size ( $\mu\text{m}$ , diameter)
10x	Olympus	0.3	656 x 1168	320	Indian Muntjac Cells	~12
100x	Olympus	1.3	80 x 81	50	Chicken RBC Nuclei	~4

**Table 1:** Microscope objective parameters and the intended imaging specimen.

prevent artifacts from forming during 3D reconstruction. Projection images at each perspective are registered with a phase-correlation-based algorithm [25]. Next, locations of the cell pixels within each registered projection image are identified, and background pixels are removed. This is done in order to preserve as much original information as possible when performing background removal. Finally, a filtered back-projection algorithm [26] is employed for tomographic reconstruction. The reconstructed cross-sections are then imported into Volview (Kitware, Inc., NY) for volume rendering. Volume rendering can provide clear definition of individual cells, and is useful for visualizing the spatial relationships between cells.

## Results

Chicken RBC nuclei (~4  $\mu\text{m}$ ) are sparsely packed inside a 50  $\mu\text{m}$  capillary tube for imaging. Multiple images are taken along a 350  $\mu\text{m}$  section of the capillary tube. The images are registered using the aforementioned algorithms, and the result is shown in Figure 2. The capillary tube wall can be seen as two horizontal lines in white. No structure can be observed in the RBC nuclei but chromosomal features in larger cells have been resolved [23]. 3D Volume rendering of the same data is shown in Figure 3. Here, background removal prior to reconstruction removes the capillary wall as well as grease on the objective, seen as repeated background patterns in Figure 2. It also successfully removes the grey background, as well as all pixels that are not identified as cells.

Volume rendering of Muntjac cells using Volview is shown in Figure 4. Muntjac cells (~12 $\mu\text{m}$ ) are tightly packed inside the 320  $\mu\text{m}$  capillary tube. The capillary tube wall can be observed as a grayish cylindrical tube around the cells. In this case, the capillary wall was not removed to provide a sense of scale. The cells aggregate in the middle of the capillary, occupying 192  $\mu\text{m}$  of the capillary diameter. Figure 4 shows approximately 600  $\mu\text{m}$  of the 1168  $\mu\text{m}$  section of the capillary imaged, which was within a single field of view. Therefore, no registration was necessary.

## Discussion

We have used different objective power and capillary sizes to show that multi-cell 3D imaging with OPTM can be achieved. Using a smaller diameter capillary, we showed that volume rendering of registered images can be successfully done (Figures 2,3). Additionally, even in densely packed sample that is 192  $\mu\text{m}$  in diameter (Figure 4), optical penetration is not limited at these specimen sizes.

Typically, practitioners use 0.413 mm ID (22 G) or smaller needles and a 20-mL syringe for fine needle aspiration [1,27]. The 320  $\mu\text{m}$  diameter capillary used in this study corresponds to a 23-gauge needle (0.337 mm ID). Glehr et al. [1] report that depending on the type of syringe used, the median total number of cells over 15 FNA aspirations was found to be anywhere from 59,680 cells/mL to 396,400 cells/mL.

Figure 4 illustrates how multi-cell OPTM imaging has the capacity

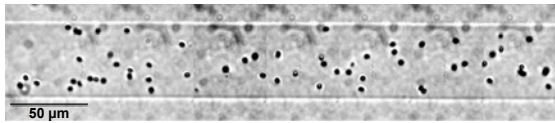


**Figure 2:** Registered image of chicken blood nuclei inside 50 μm capillary tube. A series of images are taken along the sample and registered together during post-processing. Identical patterns of grease and dirt on the objective lens can be observed in each image.



**Figure 3:** Volume rendering of Figure 2 using Vol view. Image background is removed after image registration. Here, the volumes are shown with color, which can be adjusted in software.

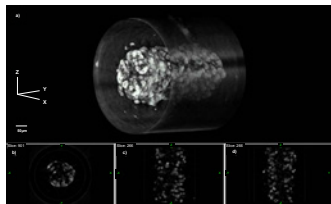


**Figure 4:** Volume rendering (a) and slices (b, c, d) of one field of view of Muntjac cells stained with hematoxylin inside a 320 μm ID capillary tube as seen under 10x objective, rendered using Volview. Reconstruction can be rotated to be seen in any orientation. Slices can be obtained along the xy (b), xz(c), and yz(d) planes.

to image a high density of cells that can represent an FNA specimen. In Figure 4, an average of 24 cells appears on each slice. Since each cell is approximately 12 μm in diameter, we can approximate that there are 24 cells per 12 μm section of the capillary. This corresponds to 24 cells per 0.347 nL, or 69 million cells/mL. The cells packed inside this microcapillary are 83 times denser than the aspirates acquired by the FNA syringe, which yields up to 396, 400 cells/mL [1]. The difference in the two densities is explained by the fact that FNA aspirates can contain blood, extracellular fluid, fat, and other biological components, while the simulated FNA was packed with cells grown from cell culture.

In Figure 4, cells aggregate at the center of the capillary tube while the gel stays near the outer walls of the capillary. In addition, since a generous amount of gel is embedded inside the capillary tube along with the cells, the packing density is relatively low and a greater packing density can be achieved. A spherical cell of 12 μm diameter occupies 905 μm<sup>3</sup> of volume, while the capillary tube has a volume of 80425 μm<sup>3</sup> per μm along its central axis. Therefore, 89 cells can be packed into every micrometer along the capillary, achieving a theoretical maximum density of 89 cells per 0.08 nL, or 1.11 billion cells/mL. Therefore, we conclude that the OPTM has more than enough capacity to image FNA samples.

Let us assume that a conventional FNA needle biopsy yields a median cell count of approximately 75,000 cells (1.25mL of sample). The length of capillary needed to image all 75,000 cells depends on the anticipated packing density. In Figure 4, cells are tightly packed, achieving a density of 69 million cells/mL. At this density, only 1.1 μL of volume is needed to pack all 75,000 cells. When the cells occupy 192 μm diameter of the capillary, we would need 38 mm of microcapillary to image all 75,000 cells. To image 38 mm of the capillary with a

FOV of 1168 μm, roughly 35 sections along the capillary need to be registered. This can be easily accomplished with the image registration algorithm used to obtain Figure 2. Unfortunately, the imaging window in our prototype OPTM instrument is limited to roughly 1500 mm. This is due to the limited range of motion of the motorized stage and the small viewing window of the cartridge which houses the capillary. In the future, the imaging window can greatly extended by making modifications to both the stage and the cartridge. On the other hand, at maximum packing density of 1.11 billion cells/mL, only 0.068 μL of volume is needed to pack all 75,000 cells. When cells occupy the full diameter of the 320 μm capillary, only 0.8 mm of the capillary is needed to image all 75,000 cells, which is smaller than the field of view of the 10x objective. Thus, depending on the packing density and capillary size, the current set-up of OPTM has the capacity to image every cell aspirated from an FNA at once.

Thicker specimen sizes of 0.2 mm in diameter are at the optical penetration limit of high-resolution optical microscopy in transmission mode. To extend optical penetration depths in thicker tissue specimens, optical clearing agents will need to be applied during sample preparation. These chemical agents have been demonstrated to decrease optical scattering in tissue, thus increasing optical penetration depths by 10 to 15 times [28]. By adding optical clearing during sample preparation, OPTM imaging of much greater specimen sizes are possible. Thus, we expect to extend this new method to CNB specimens in the future.

## Conclusion and Future Work

In this study, we have demonstrated the utility of our OPTM system in performing 3D multi-cell imaging. Densely packed cells inside the 320 μm capillary, which represents a model of FNA specimens in a 23-gauge needle, are successfully imaged and displayed in a volume rendering software. The software can display both volumetric rendering and 2D slices of the specimen, which are more familiar to clinicians.

3D imaging may provide a more intuitive and informative means to visualize FNA biopsy specimens compared to current cytologic methods; it can provide structural details of tissue organization not available on 2D cytologic smears or monolayer cell preparations. By visualizing the entire biopsy sample, the diagnostic errors resulting from cell overlap, fixed focus, absence of tissue micro-architectural information, and sampling errors can be reduced. With 3D imaging, it is possible to further increase the diagnostic accuracy of FNA biopsies.

In the future, we will modify our OPTM set-up to extend the imaging window so up to 30mm of capillary can be imaged. We will increase the imaging resolution by using 40x objectives, so specimens can be visualized in greater detail. We will compare the sensitivity and specificity of FNA biopsy using the standard 2D methods versus the new method of 3D imaging of entire FNA samples. We will also incorporate optical clearing during sample preparation and attempt to image thin CNB samples to show the possibility of performing 3D histology using OPTM. Since biopsies and imaging are both performed inside a cylindrical tube, it may be possible to perform sample preparation, including fixing, staining, washing and optical clearing, within a micro fluidics chamber, without direct handling by human operators.

## Acknowledgements

Authors would like to thank Sarah Shimer and Nitin Agarwal of the HPL for their assistance in sample preparation and with OPTM imaging. Author also want to thank members of VisionGate, Inc., especially Christy Lancaster and Ryland Bryant, for their technical assistance. Dr. Melissa Upton was a reader of this

manuscript. This project is supported by NSF grants CBET-1212540 and 1014976, and by the Washington Research Foundation.

## References

1. Glehr M, Leithner A, Gruber G, Wretschitsch P, Zacherl M, et al. (2010) A New Fine-Needle Aspiration System. *Surg Innov* 17: 136-141.
2. Shabaik A, Lin G, Peterson M, Hasteh F, Tipps A, et al. (2011) Reliability of *Her2/neu*, estrogen receptor, and progesterone receptor testing by immunohistochemistry on cell block of FNA and serous effusions from patients with primary and metastatic breast carcinoma. *Diagn Cytopathol* 39: 328-332.
3. Nagira K, Yamamoto T, Akisue T, Marui T, Hitora T, et al. (2002) Reliability of fine-needle aspiration biopsy in the initial diagnosis of soft-tissue lesions. *Diagn Cytopathol* 27: 354-361.
4. Yu YH, Wei W, Liu JL (2012) Diagnostic value of fine-needle aspiration biopsy for breast mass: a systematic review and meta-analysis. *BMC Cancer* 12: 41.
5. Berner A, Davidson B, Sigstad E, Risberg B (2003) Fine-Needle Aspiration Cytology vs. Core Biopsy in the Diagnosis of Breast Lesions. *Diagn Cytopathol* 29: 344-348.
6. Stewart CJ, Coldewey J, Stewart IS (2002) Comparison of fine needle aspiration cytology and needle core biopsy in the diagnosis of radiologically detected abdominal lesions. *J Clin Pathol* 55: 93-97.
7. Minai OA, Dasgupta A, Mehta AC, Bolliger CT, Mathur PN (2000) Interventional Bronchoscopy. *Prog In Resp Res Basel Karger* 30: 66-79.
8. Hasanovic A, Rekhman N, Sigel CS, Moreira AL (2011) Advances in Fine Needle Aspiration Cytology for the Diagnosis of Pulmonary Carcinoma. *Patholog Res Int* 2011: 897292.
9. Erickson RA (2004) EUS-guided FNA. *Gastrointest Endosc* 60: 267-279.
10. Turner BG, Cizginer S, Agarwal D, Yang J, Pitman MB, et al. (2010) Diagnosis of pancreatic neoplasia with EUS and FNA: a report of accuracy. *Gastrointest Endosc* 71: 91-98.
11. Bocking A (1991) Cytological vs histological evaluation of percutaneous biopsies. *Cardiovasc Intervent Radiol* 14: 5-12.
12. Motegi M, Tanaka S, Tada H, Sasaki T, Hashi A, et al. (2011) Comparison of Two Sampling Procedures for Diagnosing Endometrial Carcinoma and Hyperplasia: Outpatient Tissue Biopsy Versus Cytologic Examination. *J Cytol Histol* 2: 118.
13. Renshaw AA, Pinnar N (2007) Comparison of Thyroid Fine-Needle Aspiration and Core Needle Biopsy. *Am J Clin Pathol* 128: 370-374.
14. Isler RJ, Ferrucci JT Jr, Wittenberg J, Mueller PR, Simeone JF, et al. (1981) Tissue Core Biopsy of Abdominal Tumors with a 22 Gauge Cutting Needle. *AJR Am J Roentgenol* 136: 725-728.
15. Wittenberg J, Mueller PR, Ferrucci JT Jr, Simeone JF, vanSonnenberg E, et al. (1982) Percutaneous Core Biopsy of Abdominal Tumors Using 22 Gauge Needles: Further Observations. *AJR Am J Roentgenol* 139: 75-80.
16. Garini Y, Vermolen BJ, Young IT (2005) From micro to nano: recent advances in high-resolution Microscopy. *Curr Opin Biotechnol* 16: 3-12.
17. Hein B, Willig KI, Hell SW (2008) Stimulated emission depletion (STED) nanoscopy of a fluorescent protein-labeled organelle inside a living cell. *Proc Natl Acad Sci USA* 105: 14271-14276.
18. Huang B, Wang W, Bates M, Zhuang X (2008) Three-dimensional super-resolution imaging by stochastic optical reconstruction microscopy. *Science* 319: 810-813.
19. Juette MF, Gould TJ, Lessard MD, Mlodzianoski MJ, Nagpure BS, et al. (2008) Three-dimensional sub-100 nm resolution fluorescence microscopy of thick samples. *Nat Methods* 5: 527-529.
20. Fauver M, Seibel E, Rahn JR, Meyer M, Patten F, et al. (2005) Three-dimensional imaging of single isolated cell nuclei using optical projection tomography. *Opt Express* 13: 4210-4223.
21. Meyer MG, Fauver M, Rahn JR, Neumann T, Patten FW, et al. (2009) Automated cell analysis in 2D and 3D: A comparative study. *Pattern Recognition* 42: 141-146.
22. Miao Q, Hayenga J, Meyer MG, Neumann T, Nelson AC, et al. (2010) Resolution improvement in optical projection tomography by the focal scanning method. *Opt Lett* 35: 3363-3365.
23. Miao Q, Hayenga J, Meyer MG, Neumann T, Patten F, et al. (2011) High resolution optical projection tomographic microscopy for 3D tissue imaging. *SPIE Photonics West* 7904: 49040L-1.
24. Miao Q, Reeves AP, Patten FW, Seibel EJ (2012) Multimodal 3D imaging of cells and tissue, bridging the gap between clinical and research microscopy. *Ann Biomed Eng* 40: 263-276.
25. Kugliin CD, Hines DC (1975) The phase correlation image alignment method. *Proc IEEE Int Conf Cybernet Society* 163-165.
26. Kak AC, Slaney M (1988) Principles of Computerized Tomographic Imaging. *IEEE Press* 60-75.
27. Kocjan G, Chandra A, Cross P, Denton K, Giles T, et al. (2009) BSCC Code of Practice-fine needle aspiration cytology. *Cytopathology* 20: 283-296.
28. Tuchin VV (2005) Optical Clearing of Tissues and Blood. *SPIE Press*, Bellingham, WA.

This article was originally published in a special issue, **Fine Needle Aspiration Cytology in Disease Diagnosis** handled by Editor(s). Borislav A. Alexiev, University of Maryland Medical Center, USA